

Zonal fields as catalysts and inhibitors of turbulence-driven magnetic islands - Supplementary Material

D. Villa,¹ N. Dubuit,² O. Agullo,² and X. Garbet^{3,4}

¹⁾Max Planck Institute for Plasma Physics, Boltzmannstraße 2, 85748, Garching, Germany^{a)}

²⁾Aix-Marseille Université, CNRS, PIIM UMR 7345, Marseille, France

³⁾CEA, IRFM, F-13108 Saint-Paul-Lez-Durance, France

⁴⁾School of Physical and Mathematical Sciences, Nanyang Technological University, 637371 Singapore

(Dated: 12 December 2024)

I. EQUATIONS OF THE MODEL

$$\partial_t \psi = \{\psi, \phi\} - \frac{\Omega_i \tau_A \rho_*^2}{n} \{\psi, p_e\} + \frac{\eta}{n} \tilde{J}_{\parallel} \quad (1)$$

$$\begin{aligned} \partial_t \mathcal{W} = & -\{\phi, \mathcal{W}\} - \tau_i \Omega_i \tau_A \rho_*^2 \{\nabla_{\alpha} \phi, \nabla_{\alpha} p_i\} - u_{\parallel i} \{\psi, \mathcal{W}\} + \{\psi, J_{\parallel}\} \\ & + \rho_*^2 (\Omega_i \tau_A)^2 \mathcal{K}_1 \cdot \nabla (\tau_i p_i + p_e) + \mu \Delta_{\perp} \tilde{\mathcal{W}} \end{aligned} \quad (2)$$

$$\begin{aligned} \partial_t p_i = & -\frac{5}{3} p_i \{\psi, u_{\parallel i}\} - \{\phi, p_i\} - u_{\parallel i} \{\psi, p_i\} - \frac{5}{3} p_i \mathcal{K}_2 \cdot \nabla \phi + \frac{5}{3} \frac{1}{\Omega_i \tau_A} T_i \{\psi, J_{\parallel}\} \\ & - \frac{5}{3} \Omega_i \tau_A \rho_*^2 (\tau_i p_i \mathcal{K}_2 \cdot \nabla T_i - T_i \mathcal{K}_2 \cdot \nabla p_e) + \chi_{\perp i} \Delta_{\perp} \tilde{T}_i + \chi_{\parallel i} \{\psi, \{\psi, \tilde{T}_i\}\} \end{aligned} \quad (3)$$

$$\begin{aligned} \partial_t p_e = & -\frac{5}{3} p_e \{\psi, u_{\parallel e}\} - \{\phi, p_e\} - u_{\parallel e} \{\psi, p_e\} - \frac{5}{3} p_e \mathcal{K}_2 \cdot \nabla \phi \\ & + \frac{5}{3} \Omega_i \tau_A \rho_*^2 \mathcal{K}_2 \cdot \nabla (T_e p_e) + \chi_{\perp e} \Delta_{\perp} \tilde{T}_e + \chi_{\parallel e} \{\psi, \{\psi, \tilde{T}_e\}\} \end{aligned} \quad (4)$$

$$\partial_t n = -\{\phi, n\} - n \{\psi, u_{\parallel e}\} - u_{\parallel e} \{\psi, n\} - n \mathcal{K}_3 \cdot \nabla \phi + \Omega_i \tau_A \rho_*^2 \mathcal{K}_3 \cdot \nabla p_e + D \Delta_{\perp} \tilde{n} \quad (5)$$

$$\partial_t u_{\parallel i} = -\{\phi, u_{\parallel i}\} - \left\{ \psi, \frac{u_{\parallel i}^2}{2} \right\} - \frac{(\Omega_i \tau_A)^2 \rho_*^2}{n} \{\psi, \tau_i p_i + p_e\} + U_d \Delta_{\perp} \tilde{u}_{\parallel i} \quad (6)$$

where ψ is the poloidal magnetic flux, ϕ the electrostatic potential, p_e and T_e the electron pressure and temperature, p_i and T_i the ion pressure and temperature, n the electron density (quasi-neutrality is assumed) and $u_{\parallel i/e}$ the ion and electron parallel fluid velocities, with $u_{\parallel e} = u_{\parallel i} - \frac{J_{\parallel}}{n \Omega_i \tau_A}$. The definition of the generalized vorticity is

$$\mathcal{W} = \Delta_{\perp} (\phi + \tau_i \Omega_i \tau_A \rho_*^2 p_i) \quad (7)$$

meaning that here the Boussinesq approximation is applied, and imposes a condition for the equilibrium pro-

files, which is always satisfied in simulations unless clearly stated: $\partial_x \phi_{eq} = -\Omega_i \tau_A \rho_*^2 \frac{\partial_x p_{ieq}}{n_{eq}}$. Applying the Boussinesq approximation means that when evaluating the term $\nabla \cdot (n \mathbf{u}_{pol})$ the density is considered as constant everywhere it appears (including the diamagnetic drift appearing in \mathbf{u}_{pol}). The parallel current density is $J_{\parallel} = \Delta_{\perp} \psi$. A “ \sim ” above the symbol of the field indicates that only the fluctuating part of the field is retained. α in Eq. 2 is an index for the sum over the perpendicular geometrical coordinates, since the explicit expression of the second term on the RHS of Eq. 2 is: $\{\nabla_{\alpha} \phi, \nabla_{\alpha} p_i\} = \{\partial_x \phi, \partial_x p_i\} + \{\partial_y \phi, \partial_y p_i\}$. The curvature is $\mathcal{K} = (\frac{1}{B} \nabla \times \mathbf{b} + \nabla (\frac{1}{B}) \times \mathbf{b})$, with $\mathbf{b} = \frac{\mathbf{B}}{B}$. Note that the model explicitly depends on the electronic

^{a)}Electronic mail: daniele.villa@ipp.mpg.de

$$\begin{aligned}
n &= n_0 n_N \\
B &= B_0 B_N \\
u_{\parallel} &= v_A u_{\parallel N} \\
\nabla_{\perp} &= L_{\perp}^{-1} \nabla_{\perp N} \\
\nabla_{\parallel} X_N &= L_{\perp}^{-1} \{ \psi_N, X_N \} - L_z^{-1} \partial_z X_N \\
\partial_t &= \tau_A^{-1} \partial_t N \\
\psi &= B_0 L_{\perp} \psi_N \\
\phi &= B_0 L_{\perp} v_A \phi_N \\
\tau_i &= T_i / T_e \\
T_0 &= T_{0e} + T_{0i} = \frac{T_0}{1+\tau_i} + \frac{\tau_i T_0}{1+\tau_i} \\
\Omega_i &= e B_0 / m_i \\
\rho_*^2 &= \frac{T_{0e}}{m_i} \frac{1}{\Omega_i^2} \frac{1}{L_{\perp}^2} = \frac{T_0}{m_i} \frac{1}{\Omega_i^2} \frac{1}{L_{\perp}^2} \frac{1}{1+\tau_i} = \frac{\beta_{e0}}{2n_0} \\
\beta_{e0} &= 2(\Omega_i \tau_A)^2 \rho_*^2 \\
p_e &= \frac{p_0}{(1+\tau_i) \rho_*^2 \Omega_i \tau_A} p_{eN} \\
p_i &= \frac{p_0 \tau_i}{(1+\tau_i) \rho_*^2 \Omega_i \tau_A} p_{iN} \\
\mathcal{K}_3 &= \mathcal{K}_2 = -(5/3) \rho_*^2 \mathcal{K}_1
\end{aligned}$$

TABLE I. Normalization used for the equations of the model. Quantities with subscript “0” are reference values at the resonant surface. $v_A = \frac{c B_0}{\sqrt{m n_0}}$ is the Alfvén velocity at resonant surface. L_{\perp} is a characteristic perpendicular length of the system. \mathcal{K}_3 and \mathcal{K}_2 are parameters introduced to manipulate linear spectrum.

η	$1 \cdot 10^{-5}$	ρ_*^2	$1.66 \cdot 10^{-4}$
μ	$5 \cdot 10^{-4}$	\mathcal{K}_1	$-0.5 [-1]$
$\chi_{\perp e/i}$	$5 \cdot 10^{-5}$	$\mathcal{K}_2 = \mathcal{K}_3$	$-3 \cdot 10^{-1}$
$\chi_{\parallel e}$	$5.0 \cdot 10^2$	L_y	6π
$\chi_{\parallel i}$	$8.0 \cdot 10^0$	$\tau_i = T_i / T_e$	1.0
D	$1 \cdot 10^{-4}$	$\Omega_i \tau_A$	$3.12 [6.24]$
U_d	$5 \cdot 10^{-5}$	L_x	10

TABLE II. Dissipative and dimensionless parameters used for the 2D non-linear simulations in slab geometry. The value of $\Omega_i \tau_A$ in brackets is for the higher- β case. The value of \mathcal{K}_1 in brackets is for the stronger drive case.

beta through the relation $\beta_{e0} = 2(\Omega_i \tau_A)^2 \rho_*^2$
II. PARITY ANALYSIS THROUGH COMPLEX ARGUMENT DIFFERENCES

Since the paper employs an unconventional way to define the parity of the modes, using the average argument of the complex-valued functions, rather than comparing values across a center of symmetry, here is provided some more insight on this point. Fig. 1 shows the eigenfunctions of two different simulations in the linear phase: one interchange unstable (shown with circles), the other tearing unstable (shown with empty squares). The left-axis shows the normalized absolute value of the mode, while the colorscale shows the difference between the phase of the function at any given radial position to the phase of the function at a chosen radial position (in this case the $x = 0$ position). Note that the slight asymmetry in the

absolute value of the interchange unstable mode is an effect due to the cubic terms when the equilibrium pressure profile is not flat (in the tearing unstable simulation this profile was flat), an effect that will be investigated in a paper currently in preparation. As evident, an even mode (i.e. an unstable tearing mode) has constant phase across the resonant position, whereas the interchange unstable mode has a phase change of $\pi/2$ across the resonant position. In these linear simulations, these phase differences will be exact, as is evidenced by the average values $\langle |\Delta\varphi|/2\pi \rangle$ computed and shown in Fig. 1. In the non-linear simulations of the paper, these averaged values will not be exact as is the case in this linear example, but lower average phase differences indicate a more relevant tearing parity of the mode, whereas higher values indicate dominant interchange parity (i.e. that parity of the mode changes more across the radius, as is the case in the interchange parity simulations).

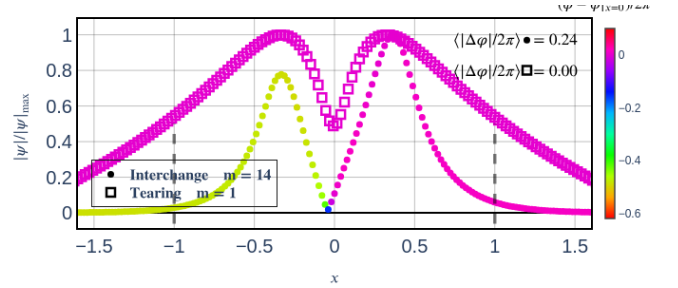


FIG. 1. Comparison of the linear modes for two different simulations: one interchange unstable (shown with circles), the other tearing unstable (shown with empty squares). The asymmetry in the absolute value of the interchange unstable mode is due to the cubic terms.

III. THE COALESCENCE PROCESS

Here are shown some figures to illustrate the difference between simulations that show coalescence (weaker magnetic shear $\partial_x B_{eq} = 0.01$ and slightly stronger instability drive $\gamma^* = 0.018$) and those that don't (stronger magnetic shear $\partial_x B_{eq} = 0.02$ and slightly weaker instability drive $\gamma^* = 0.015$). These simulations were not directly used in the paper, but clearly illustrate the different behaviours of the two regimes, while also having very similar instability drives, thus highlighting the role of the shear in the dynamics. Using the isocontours of the magnetic potential ψ one can see how in the linear phase (Figs. 2 and 3) both simulations are unstable to interchange modes, with the simulation with weaker magnetic shear showing radially broader modes. In the early non-linear phase, the simulation with stronger magnetic shear (Fig. 4) retains dominant interchange parity in its modes, whereas the simulation with weaker magnetic shear (Fig. 5) has modes with noticeably more tearing-like parity. Fig. 6 shows the late non-linear phase of a simulation

that undergoes coalescence (this one part of the set used in the paper), with turbulent regions enclosed within the magnetic islands that have formed non-linearly. Fig. 7 shows the late non-linear phase of a simulation run with the same parameters as the simulation giving Fig. 6 but without including the cubic terms in the dynamics, showing their crucial role in allowing the mechanism described in the paper to take place. Figs. 8 - 12 show a sequence of isocontours for the simulation with $\gamma^* = 0.049$ and $\partial_x B_{eq} = 0.02$ (zoomed in to the region $x \in [-3, 3]$) to more clearly illustrate the merging of structures from small to large scales. Figs. 13 - 14 show a zoomed-in detail of the isocontours for two simulations in the non-linear phase, where the one undergoing coalescence can be seen having regions with fluctuations of ψ of the same sign aligning horizontally, effectively changing the parity of the mode.

Note: γ^* is the growth rate of the most unstable mode in the linear phase.

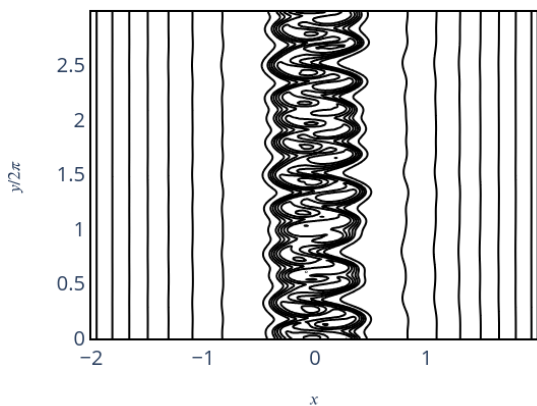


FIG. 2. Isocontours of ψ for a simulation with $\gamma^* = 0.015$ and $\partial_x B_{eq} = 0.02$, that will **not** undergo coalescence, showing interchange parity in the linear phase.

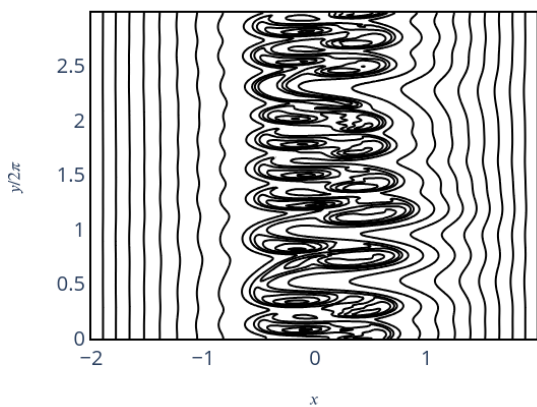


FIG. 3. Isocontours of ψ for a simulation with $\gamma^* = 0.018$ and $\partial_x B_{eq} = 0.01$, that will undergo coalescence, showing interchange parity in the linear phase.

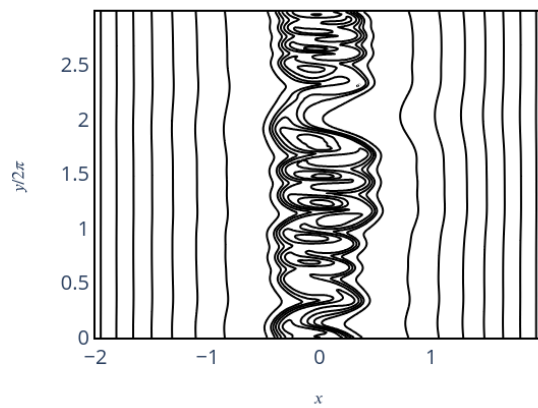


FIG. 4. Isocontours of ψ for a simulation with $\gamma^* = 0.015$ and $\partial_x B_{eq} = 0.02$, that will **not** undergo coalescence, showing interchange parity in the early non-linear phase.

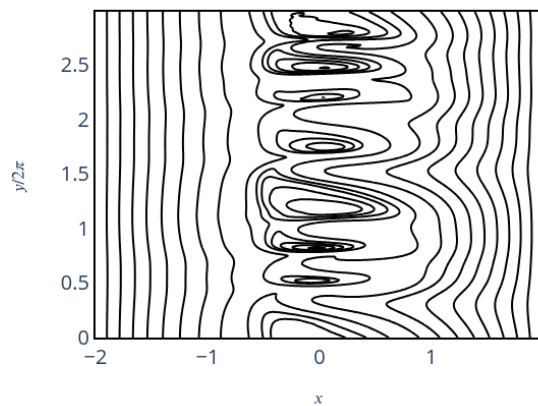


FIG. 5. Isocontours of ψ for a simulation with $\gamma^* = 0.018$ and $\partial_x B_{eq} = 0.01$, that will undergo coalescence, showing tearing-like parity in the early non-linear phase.

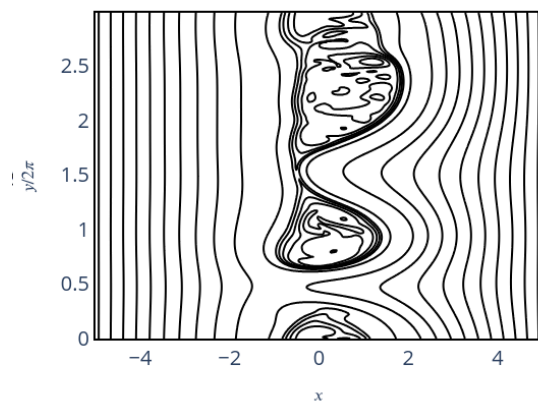


FIG. 6. Isocontours of ψ in the late non-linear phase of a simulation with $\gamma^* = 0.083$ and $\partial_x B_{eq} = 0.02$ that shows coalescence. Notice the X-points at $y \approx 3\pi$ and $y \approx \pi$.

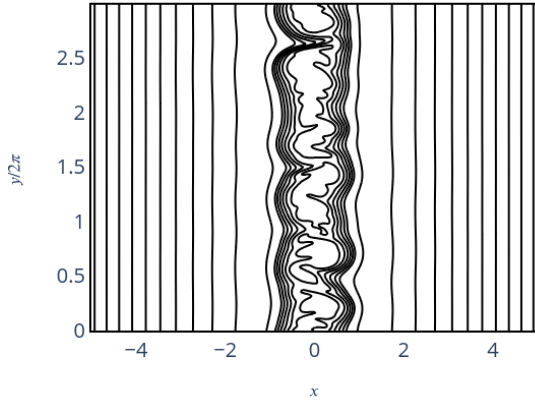


FIG. 7. Isocontours of ψ in the late non-linear phase of a simulation with $\gamma^* = 0.083$ and $\partial_x B_{eq} = 0.02$ where **the cubic terms were not included in the dynamics** (compare to Fig. 6). Notice that the modes retain interchange parity and remain limited in width.

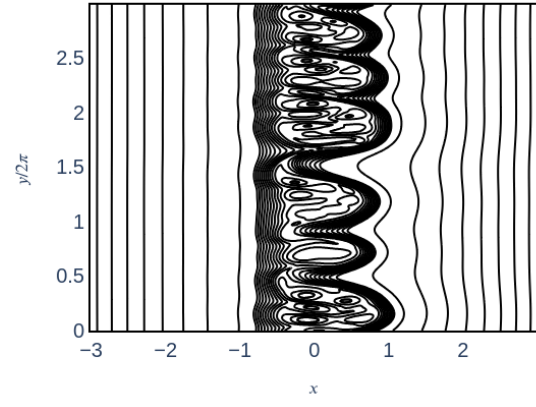


FIG. 10. Isocontours of ψ in the fully developed non-linear phase for the simulation with $\gamma^* = 0.049$ and $\partial_x B_{eq} = 0.02$.

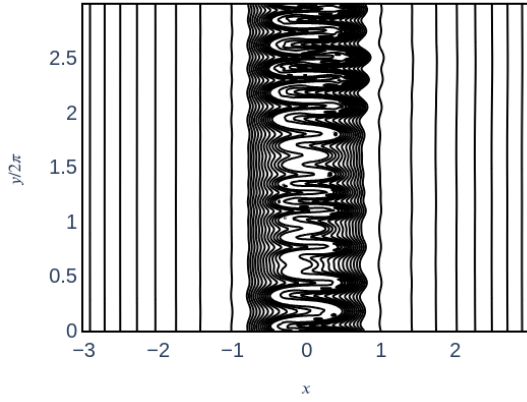


FIG. 8. Isocontours of ψ in the late linear phase for the simulation with $\gamma^* = 0.049$ and $\partial_x B_{eq} = 0.02$.

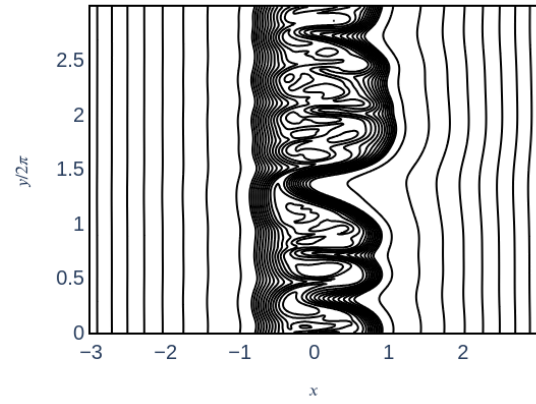


FIG. 11. Isocontours of ψ in the late non-linear phase for the simulation with $\gamma^* = 0.049$ and $\partial_x B_{eq} = 0.02$.

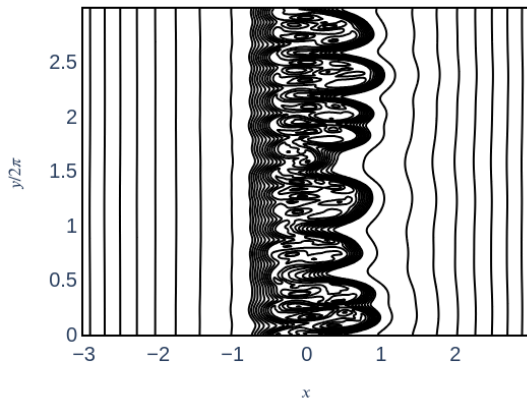


FIG. 9. Isocontours of ψ in the early non-linear phase for the simulation with $\gamma^* = 0.049$ and $\partial_x B_{eq} = 0.02$.

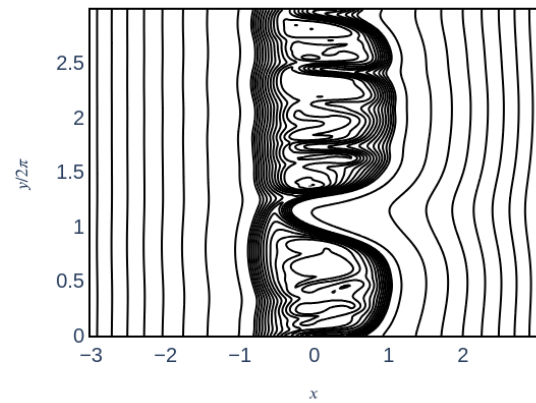


FIG. 12. Isocontours of ψ at the latest point available in the non-linear phase for the simulation with $\gamma^* = 0.049$ and $\partial_x B_{eq} = 0.02$.

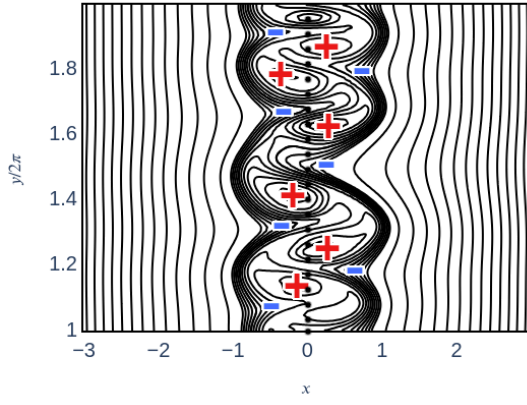


FIG. 13. Zoomed in detail of the isocontours of ψ for a simulation with $\gamma^* = 0.015$ and $\partial_x B_{eq} = 0.02$, that does **not** undergo coalescence, showing that the fluctuations of ψ (in most cases) change sign across the resonant position, maintaining a dominant interchange parity.

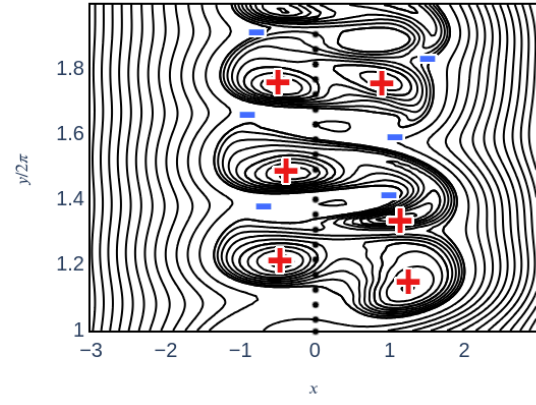


FIG. 14. Zoomed in detail of the isocontours of ψ for a simulation with $\gamma^* = 0.018$ and $\partial_x B_{eq} = 0.01$, as it is undergoing coalescence, showing how the fluctuations of ψ of the same sign tend to align horizontally, changing the phase of the mode.